ICAS 2020 SHANGHAI
International Council of the Aeronautical Sciences
32nd Congress of the International Council of the Aeronautical Sciences
September 6-10, 2021
Pudong Shangri-La, Shanghai, China

# NUMERICAL EVALUATION OF DYNAMIC STABILITY DERIVATIVES FOR HIGH LIFT DEVICES

Hamood Ur Rahman[1], Adnan Maqsood[1], Rizwan Riaz[1], and Laurent Dala[2]

[1]National University of Sciences and Technology, Islamabad, Pakistan,
[2]Northhumbria University, UK

## Abstract

This research aims to find the fundamental effects of high lift devices on the stability characteristics of a high-lift airfoil through computational fluid dynamics. Stability derivatives are calculated for four configurations: clean, slat deployed, flap deployed, and slat and flap deployed configuration. The static and dynamic coefficients are calculated by using the forced oscillation technique. Simulations are performed at various angles of attack and keeping the oscillation amplitude and frequency constant. This approach enabled the efficient and accurate computation of stability derivatives. The results indicate an improvement in static stability characteristics; however, the dynamic stability deteriorates with the deployment of high-lift devices.

**Keywords***:* high-lift, stability, CFD, pitch moment damping

## 1. Introduction

High lift devices (HLD) are wing surfaces that change the aerodynamic characteristics for desirable performance in a specific flight regime. They improve the slow flight performance and help to reduce the stall speed by increasing the maximum lift coefficient [1]. Different types of high lift systems are operational in the aviation industry [2]; the most common of them include flaps and slats. These conventional HLDs are being used on airplanes for several decades and have been optimized extensively, with only modest improvements in aerodynamic performance being possible. When high-lift devices are deployed, the aerodynamic force distribution over the airfoil changes [3], consequently changing the position of the aerodynamic center affecting the stability of aircraft. Some other methods, primarily given attention by the research community, include high lift generation through power augmentation [4] in transport aircraft, blowing and suction used to delay stall and [5], vortex generation [6], Magnus effect [7], and plasma actuation [8].

To have a better high-lift system design, we must understand the flow physics around a multi-element airfoil. To determine these aerodynamic characteristics, experimental procedures are costly and time-taking [9], and the analytical approach is not flexible enough [10]; therefore, researchers have turned to computational fluid dynamics (CFD) for determining aerodynamic characteristics of different flying bodies [11]. The effectiveness of CFD lies in its ability to simulate the same conditions of an experimental test as long as the approach is correct [12].

The major push during the design activity is to increase static aerodynamic performance [13]; however, stability considerations are often reported during the experimentation phase [14]. Stability Augmentation Systems (SAS) are deployed to improve flight characteristics [15] to compensate for any undesirable phenomena. CFD can be employed to determine the pitch damping coefficients [16], [17] like experimental procedures in wind tunnels and test flight ranges. Advancement in numerical tools like CFD has made it possible to analyze the flow around high-lift devices and to have a deep understanding of the flow phenomena.

In this paper, the longitudinal pitch moment damping characteristics of TC12 airfoil with HLDs are evaluated. Initially, experimental data of NACA 0012 airfoil carried out by Landon [18] is used to validate the computational setup.

Subsequently, the effects of the slat and flap on damping derivatives in the longitudinal direction are explored. The quantitative variations of stability characteristics are correlated with flow physics.

## 2. Problem Formulation

### 2.1. Geometric Description

The TC12 profile [19], as shown in Figure 1, is an efficient and supercritical transonic airfoil designed by Airbus for researching at transonic cruise regimes. The profile also has a high lift configuration intended for take-off and landing. The high lift configuration consists of a slat, central element, and Fowler flap (referred to from here simply as 'the flap'). These airfoil elements are shown in Figure 1, compares the clean and high lift configurations of the TC12 profile. The high lift configuration shown (with slat and flap extended) is set to the landing configuration. During this research, four different configurations will be used. These include:

a) Clean configuration.
b) Slat deployed configuration.
c) Flap deployed configuration.
d) Slat and flap deployed configuration.

Although configurations (*b)* and (*c)* are not practically used, these are considered in this research to see the individual effects of slat and flap. They are all imported to ANSYS® individually, where flow domains are constructed the same as presented in Figure 2.

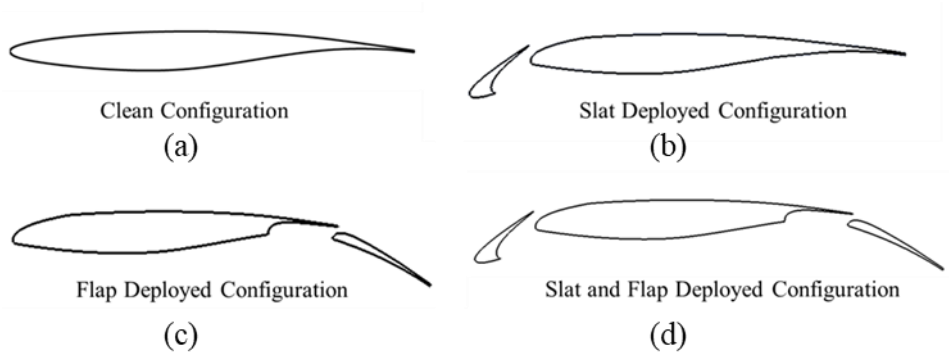


Figure 1 – Different configurations of TC12 airfoil

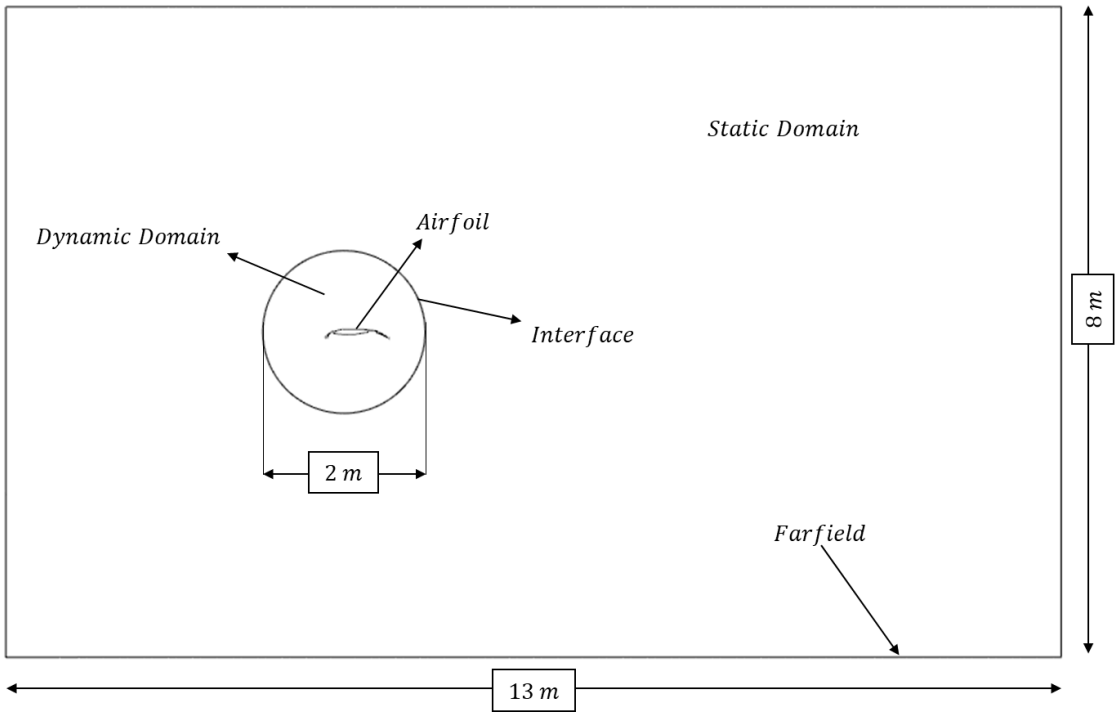


Figure 2 – Flow domain geometry around TC12 airfoil showing static domain, dynamic domain, interface and far-field along with dimensions.

## 2.2. Numerical Setup and Validation

The solution of fluid-flow problems through numerical techniques is always approximated and contains different modeling errors, discretization errors, and convergence errors. The sum of these errors gives the overall difference between experimental or analytical solutions. In this research, simulated results of lift coefficient are compared with experimental results for validation at different angles of attack of TC12 airfoil at Reynolds number of $2.95 \times 10^6$ and with Mach $0.2$. The discretized domain is shown in Figure 3. Three different turbulence models are compared with experimental data, as shown in Figure 4(a). It can be remarked that the S-A model shows better agreement with experimental results; therefore, the S-A model is used for further simulations on TC12 airfoil.

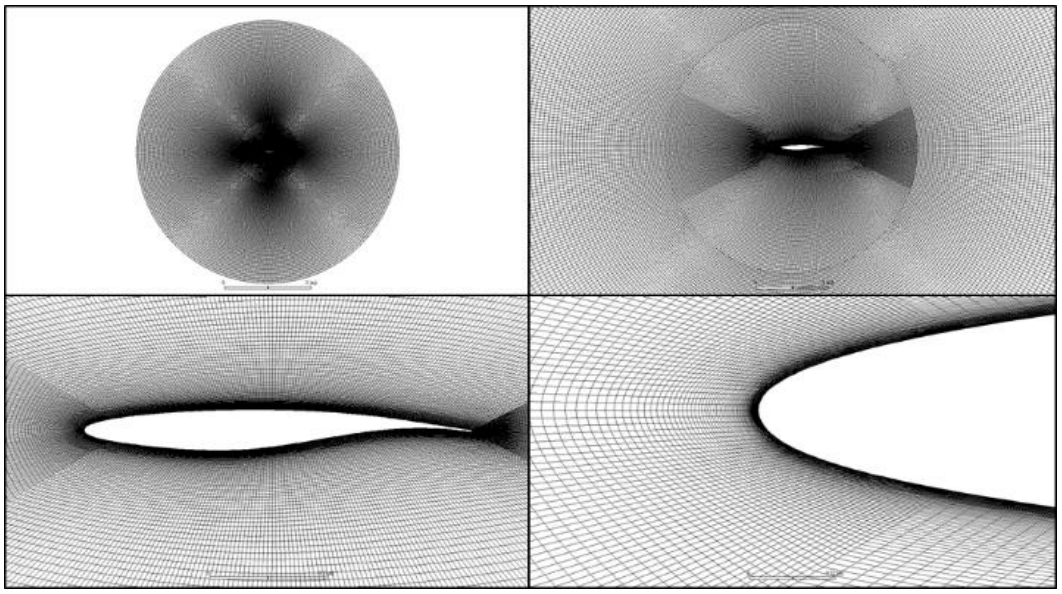

(a)

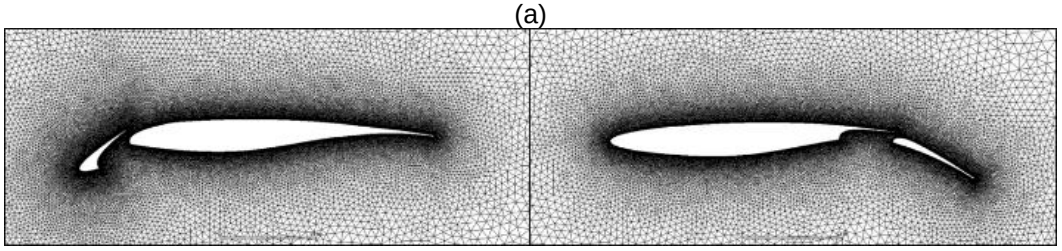

(b)

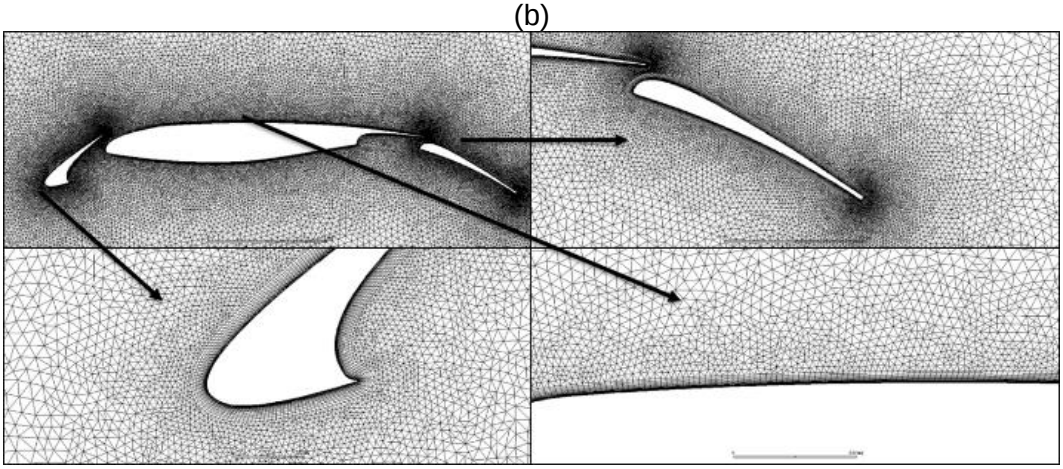

(c)

Figure 3 – (a) Grid domain of airfoil, (b) mesh with slat only, and (c) with slat and flap deployed.

Figure 4(b) compares the pressure coefficient distribution along the chord length of clean configuration with origin at quarter chord computed through S-A turbulence model [20] at 8.11° angle of attack. The results obtained through CFD are in good agreement with the experimental data. At 10°, the flow separates, and the lift coefficient drops, thereby signifying stall.

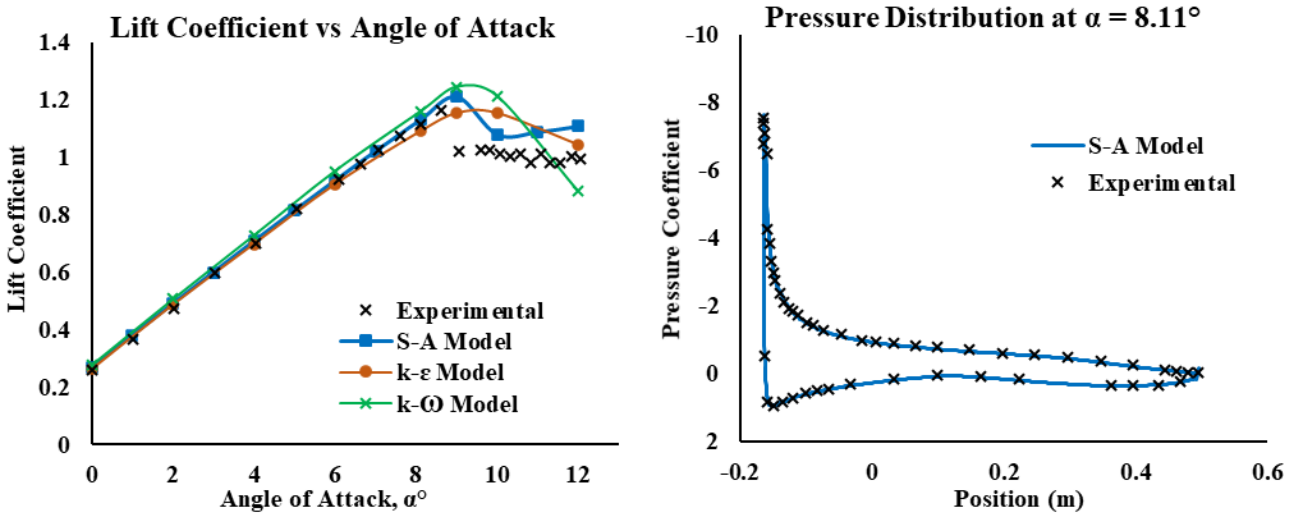


Figure 4 – (a) Lift Coefficient vs Angle of Attack for TC12 airfoil in clean configuration, (b) Pressure Coefficient along the chord length of TC12 airfoil in clean configuration at 8.11° angle of attack

Lift coefficients for the high-lift configuration of TC12 airfoil are plotted (Figure 5 (a)) against angles of attack ranging from 0° to the angle of attack where it reaches stall that is 16°. The data obtained through the S-A model is compared to experimental data for the high-lift configuration and demonstrated good agreement.

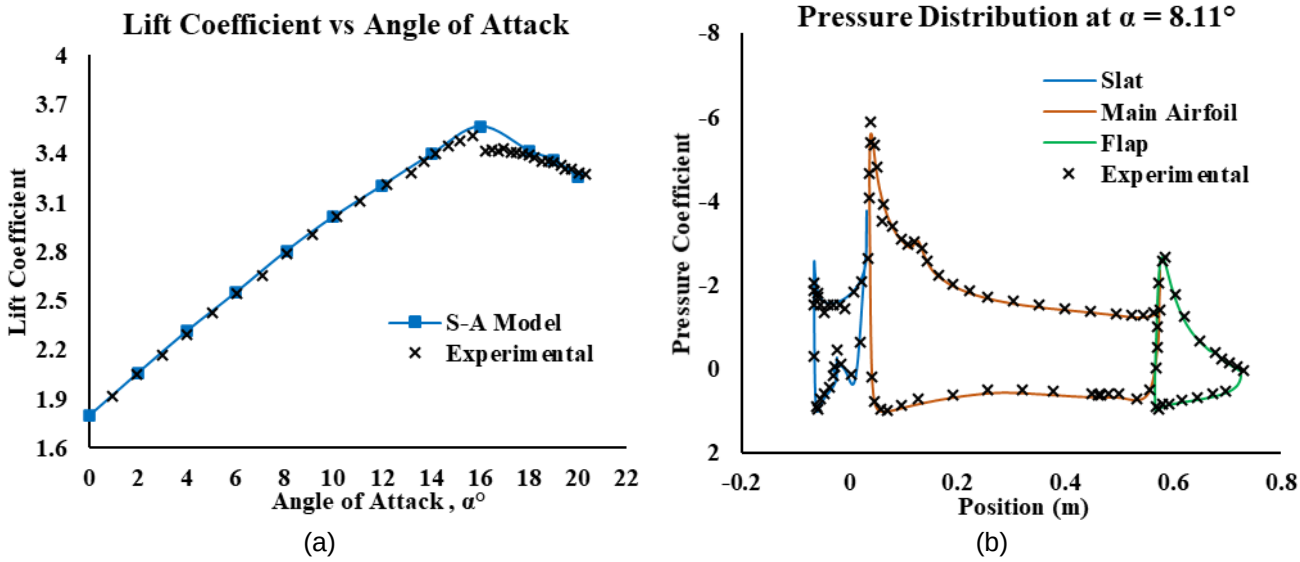


Figure 5 – (a) Comparison of lift coefficient with experimental data, (b) Pressure coefficient distribution along chord length at 8.11° angle of attack for TC12 in high-lift configuration using S-A model (slat and flap deployed configuration)

Figure 5(a) displays pressure coefficient distribution along chord length (with origin at quarter chord) computed through CFD and compared with the experimental data at an angle of attack of 8.11°. The three enclosed areas with blue, orange and green lines show pressure coefficient distribution over the slat, main element, and flap, respectively. The pressure coefficient distribution shows good agreement with experimental data through predicting major flow features on the high lift airfoil. At the main element, the pressure peak is predicted accurately, and a separation bubble on the suction surface at the leading edge around $x = 0.125\ m$ is projected. Similarly, flow separation at flap is indicated approximately at $x = 0.67\ m$, and the pressure on the slat is also predicted accurately.

## 2.3. Evaluation of Stability Coefficients

A more common and computationally efficient method for stability coefficients is the forced oscillation technique [21]. It is a single-point method that utilizes the time history data in the form of hysteresis loops. In this technique, the airfoil is forced to oscillate according to a harmonic forcing motion of small

amplitude and frequency. Mumtaz et al. [22] used this technique to derive dynamic derivatives for NACA0012 and flat plat at different mean angles of attack, while Shagufta et al. [23] derived dynamic derivatives for an airfoil with an opposing jet in a supersonic regime. The method is valid for small frequencies and amplitudes and establishes the relationship between the aerodynamic forces and the primary motion. In this method, the airfoil is given an oscillatory motion with a pivot at the center of gravity represented by Equation (1) [17]:

$$\alpha = \alpha_0 + A \sin \omega t \tag{1}$$

where $\alpha$ is the angle of attack at a given instant, $\alpha_0$ is the initial angle of attack while $A$ is the amplitude of the oscillation, and $\omega$ is the frequency of the oscillations. The angular frequency can be determined from the reduced frequency $k$ which demonstrates the level of unsteadiness [24], [25]. In this research extreme value of unsteadiness is chosen that is $k = 0.2$

$$k = \frac{\omega c}{2U_\infty} \Rightarrow \omega = \frac{2U_\infty k}{c} \tag{2}$$

From Equation (2), with the value of $k = 0.2$ , $\omega = 6.64\, rad/sec$ is obtained. This value was incorporated in UDF (User Defined Function) code in ANSYS Fluent ® [26] for stability derivatives coefficients. An optimum time step size (0.0125 sec) is obtained through time step size independence. Subsequently, the transient flow effects can be properly captured for the desired accuracy with rigorous computational resources. During this process, the step size was reduced until there was no change in the hysteresis loop, as shown in Figure 6.

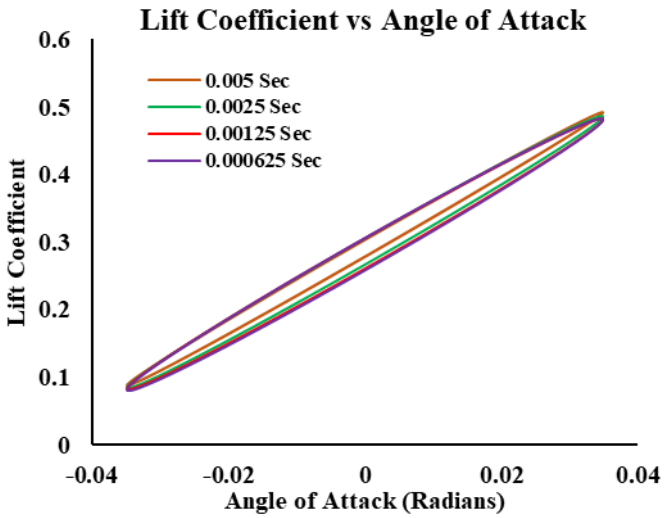


Figure 6 – Hysteresis loop of lift coefficient vs angle of attack for different time step sizes

The stability derivatives of interest in the present analysis are those in the pitching degree of freedom, but these can be derived in lateral and yaw direction. Umer et al. [27] evaluated flight dynamics characteristics for a small-scale morphing capable UAV in the longitudinal and lateral direction. The motion in the pitch direction is a function of both static and dynamic stability derivatives [17]. The static pitch stability coefficient, $C_{m_\alpha}$, arises due to changing forces on the airfoil as the angle of attack is altered [28]. $C_{m_\alpha}$ is also known as pitch stiffness, and it acts like a spring constant $k$ found in $m\ddot{x} + c\dot{x} + kx = 0$.

$$C_{m_\alpha} = \frac{\partial C_m}{\partial \alpha} \tag{3}$$

where $C_m$ is moment coefficient while $\alpha$ is the angle of attack in radian. If an aerodynamic object is statically stable in pitch, the slope of the $C_{m_\alpha}$ curve should be harmful [22]. This opposes any deviations and forces the airplane back towards the equilibrium position when perturbed [23]. Two dynamic derivatives contribute to dynamic pitch stability. These are the moment coefficient due to pitch rate, $C_{m_q}$, and the moment coefficient due to the rate of change of angle of attack, $C_{m_{\dot{\alpha}}}$. These expressions

are defined in terms of the angular rates $q$ and $\dot{\alpha}$ nondimensionalized by the free stream velocity and chord length, which are treated as constants in this research for each configuration. Practically, it is very challenging to measure dynamic stability derivatives coefficients due to change in $\dot{\alpha}$ and $q$ separately; therefore, it is usual to determine the sum of two known as pitch damping stability coefficient [29].

$$C_{m_q} = \frac{\partial C_m}{\partial\left(\frac{qd}{2V_\infty}\right)} = \frac{2V_\infty}{d}\frac{\partial C_m}{\partial q} \tag{4}$$

$$C_{m_{\dot{\alpha}}} = \frac{\partial C_m}{\partial\left(\frac{\dot{\alpha}d}{2V_\infty}\right)} = \frac{2V_\infty}{d}\frac{\partial C_m}{\partial \dot{\alpha}} \tag{5}$$

For the determination of stability coefficients for high-lift configuration, an experimental case study of flow over the oscillating NACA 0012 airfoil is simulated, and the results of normal force and moment coefficients are compared with experimental data in Figure 7 carried out by Landon [18]. Later, the same method is used to determine stability derivatives of TC12 Airfoil for configurations at different mean angles of attack.

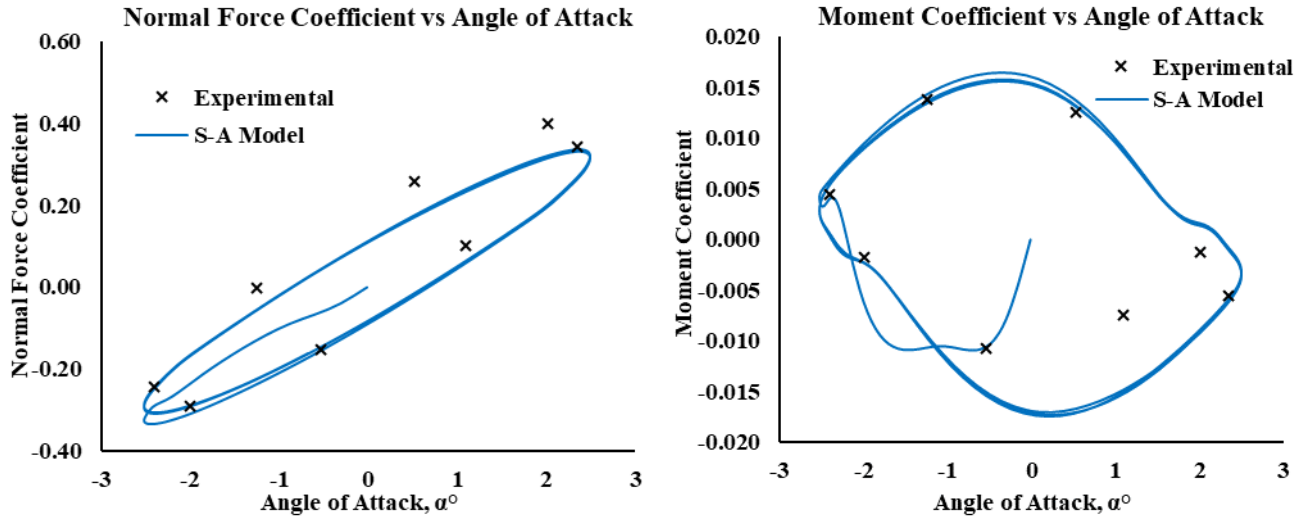


Figure 7 – (a) Normal Force Coefficient and (b) Moment Coefficient vs Angle of Attack for NACA 0012 (Comparison with Experimental Data)

## 3. Results and Discussions

### 3.1. Steady Case

The steady case results of clean configuration are simulated and validated by comparing them to the experimental data. The same methodology is extended to simulate the flow over the remaining configurations, and the results of lift and drag coefficients are plotted in Figure 8.

It is observed in Figure 8 that when the flap is deployed, the lift coefficient is increased, and the stall occurs a little earlier as compared to the clean configuration due to the gap between the flap and main airfoil. Flap deployment also causes drag to increase earlier as the angle of attack is increased because the flap angle of attack is greater than the main airfoil, and flow separation occurs much earlier on the flap than the main airfoil.

When the slat is deployed, the stall has been delayed from 9° to 22° angle of attack because of new energetic boundary layer formation at the trailing edge of the slat. Here, the slat is not performing well at low angles of attack because of the flow separation at the lower side of the slat at the cove. At lower angles of attack, the slat has higher drag. Still, it decreases when the flow re-attaches to the airfoil as the angle of attack increases from 0° to 4° and then again starts to grow because of the increase in induced drag in the direction of airflow over the airfoil.

When both slat and flap are deployed, the lift coefficient increases and the stall is delayed. Here, in this case, slat and flap showcase their advantages. The flap increases lift, and at the same time, the slat keeps the flow attached to the airfoil, causing the stall to delay. It can also be observed that at lower angles of attack, the lift coefficient in the case of both slat and flap deployed is a little lower than the

only flap deployed configuration. This is because the slat negatively impacts the lift coefficient because of flow separation on the lower side. We can observe higher drag due to increased overall surface area of the airfoil and comparatively early flow separation at flap. Again, the stall occurs earlier than the slat-only configuration due to the gap among the slat, main airfoil, and flap. Therefore, considering the results in Figure 8, it is concluded that each element has its significance and can be used in specific flight regimes as per requirement.

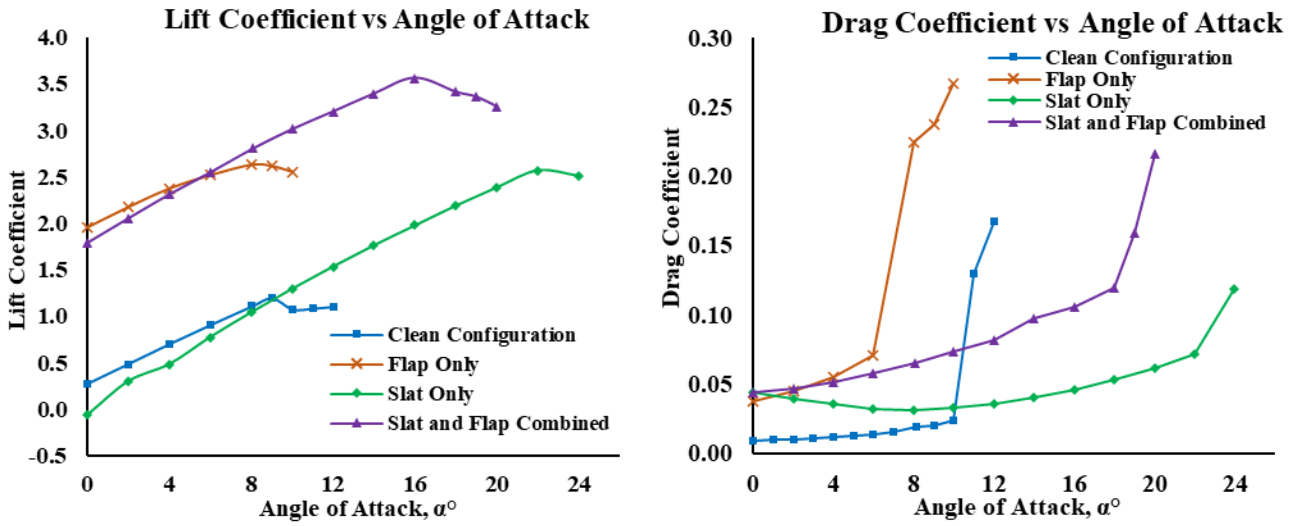


(a) (b)

Figure 8 – (a) Lift and (b) drag coefficient vs angle of attack for four different configurations of TC12 airfoil.

## 3.2. Static Stability

The simulation results for static stability coefficients for different configurations are presented in Figure 12(a). These static stability derivatives' coefficients are derived through forced oscillation with quarter chord as pivot point. The moment coefficient vs. pitch angle is plotted, and a hysteresis loop is formed. The slope of this hysteresis is approximated through linear least square approximation, which represents the static stability derivative coefficient. This procedure is repeated for all configurations and at different mean angles of attack.

### *3.2.1. Clean Configuration*

For clean configuration, the flow remains attached to the airfoil at mean angles of attack of $-8°$ to $+8°$. The pitching moment graphs show no disturbances in the loop, as shown in Figure 9 (a). However, at 12° mean angle of attack, the flow over the airfoil entirely separates, causing a stall. The linear estimation through the forced oscillation technique is not valid for the derivation of stability derivatives' coefficients. For the post-stall regime, the *near-field* and *far-field methods* are used [28]. At all the simulated mean angles of attack, the slope values are positive given in Figure 12(a) because the force distribution is such that the aerodynamic center remains ahead of the center of rotation. Therefore, if the airfoil in a clean configuration is perturbed, it will not tend to return to its equilibrium position. Hence there is a need for the stabilizer to counter this disturbance.

### *3.2.2. Flap Deployed Configuration*

When the flap is deployed, the values of static stability coefficients are positive at negative mean angles of attack. Here, the flow remains attached to the airfoil. The force distribution is such that the aerodynamic center is ahead of the moment center and separation bubble appearance at the flap's leading edge due to less energetic boundary flow on the lower side of the airfoil. But as the mean angle of attack is increased, the aerodynamic center moves behind the moment center because of the disappearance of separation bubble at the leading edge of the flap and more lift force generated by the flap causing the slope of the moment coefficient to be negative. A negative value of the static stability coefficient indicates that the airfoil will return to its equilibrium position if perturbed. The flow remains attached until 4°, and there are no disturbances in flow and remains laminar. When the mean angle of attack reaches 6°, the flow separates every second cycle, as illustrated in Figure 9(b).

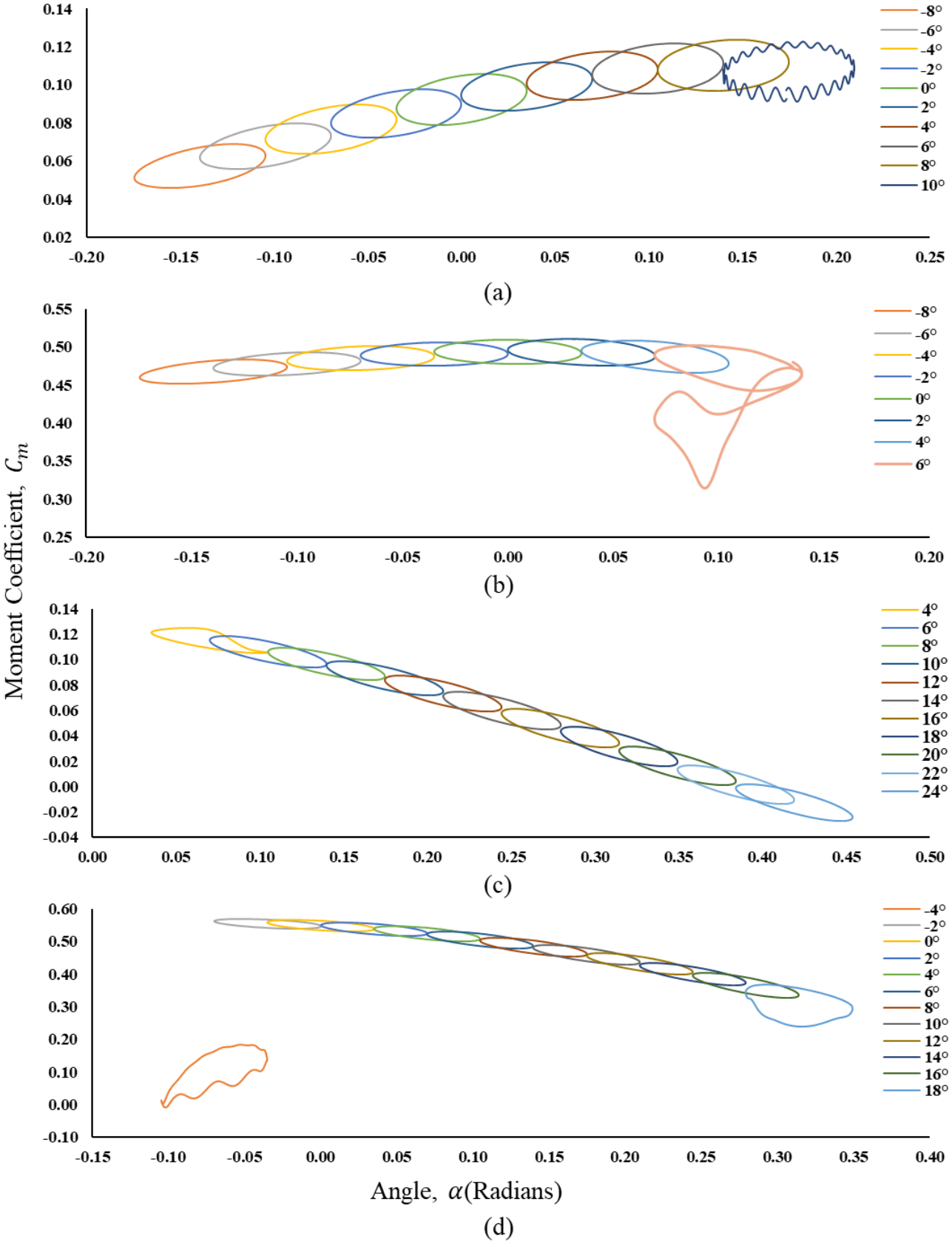


Figure 9 – Moment coefficients vs mean angles of attack (in radians) for (a) clean configuration (b) flap deployed configuration (c) slat deployed configuration (d) slat and flap deployed configuration.

### *3.2.3. Slat Deployed Configuration*

The slat is a leading-edge device deployed at higher angles of attack to keep the flow attached to the airfoil; however, it reduces the performance at lower angles of attack because of detached flow on the

lower surface of the airfoil. At a 4° mean angle of attack, the flow starts reattaching to the airfoil. During the oscillation, the vortex bubble at the slat's cove changes sizes with a change in pitch angle, as evident from the moment coefficient vs. angle of attack in Figure 9(b). The moment coefficient graph is not uniform, but the overall slope of the graph remains negative, indicating static stability. The flow remains attached to the airfoil from 6° to 24° mean angles of attack; however, there is a vortex bubble at the slat's cove which does not fluctuate over the airfoil and in the slot. At 26°, the flow separates on the upper surface of the slat, and the airfoil goes in the post-stall regime. When slopes are derived by plotting moment coefficient vs. pitching angle, all the pitches have negative values plotted in Figure 9(c), proving the configuration to be statically stable if perturbed.

### *3.2.4. Slat and Flap Deployed Configuration*

When both slats and flaps are deployed, at $-4°$, the configuration is statically unstable as the value of the slope is positive. It can be observed from the graph in Figure 9(d), the moment coefficient fluctuates during the upward rotation of the airfoil due to the vortex shedding from the airfoil resulting in instability. As the angle of attack increases, the bubble at the cove becomes stables and does not detach during the oscillations of the airfoil causing the airfoil to become stable. When the mean angle of attack reaches 18°, a leading-edge vortex formation starts during the upstroke. It disappears during the downward rotation, but it has only little effect on the slope of the graph, which remains negative. From Figure 9, slopes at all mean angles of attack are negative, proving that airfoil will tend to return its equilibrium position when both slat and flap are deployed, hence statically stable. Another observation is that this configuration's slope magnitudes are more negative than other configurations proving that it has a higher tendency to come back to its equilibrium position, proving more static stability.

These analyses are carried out at different mean angles of attack as these high-lift configurations are operated during different flight regimes. For example, only flap deployed configuration has better performance at lower angles of attack while the slat has better performance at higher angles of attack.

To conduct a comparative analysis of the HLDs, static and dynamic stability graphs have been plotted in Figure 10 at the same mean angle of attack of $4°$. It can be observed that the clean configuration has a positive slope making it statically unstable at this mean angle of attack. While the slopes for the configurations with an HLD are negative when approximated through the linear least square method indicating static stability. Their pressure distribution is such that the aerodynamic center lies behind the center of gravity, making it inherently statically stable at this mean angle of attack. While the slopes for all the configurations are positive (Figure 10), they will not come to equilibrium; instead, their amplitude will increase over time.

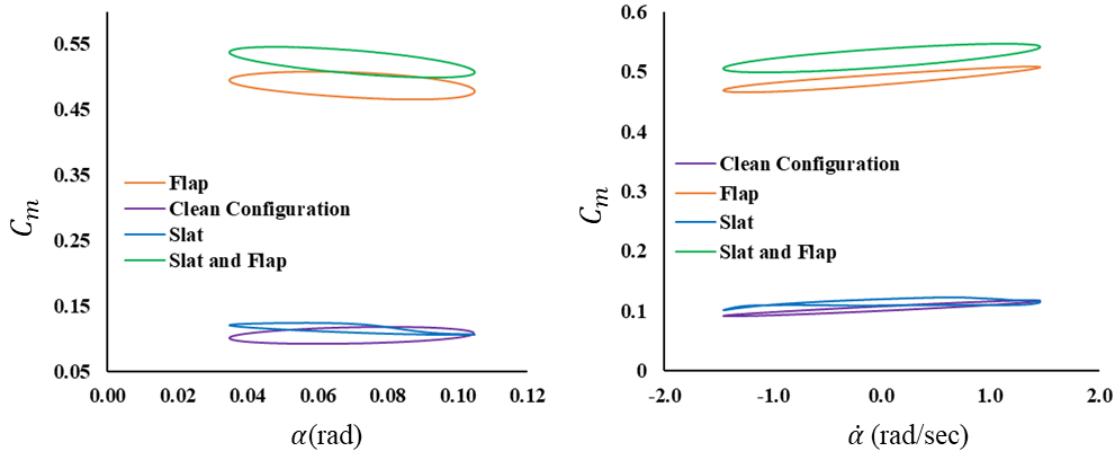


(a) (b)

Figure 10 – (a) Moment coefficient vs pitching angle (rad), (b) Moment coefficient vs pitching rate (rad/sec) at $\mathbf{4}°$ mean angle of attack

## 3.3. Dynamic Stability

The analysis of dynamic stability derivatives' coefficient, also known as pitch damping coefficient, is derived by taking the derivative of moment coefficient with respect to the non-dimensionalized rate of pitch angle change. It is determined by plotting the moment coefficient vs. rate of change of pitch angle

($\alpha$) and then non-dimensionalize it. The slope found through the least square approximation method is the damping coefficient. This value can tell the time history of disturbance. If the value of the slope is positive, the disturbance will increase with time, and when the value of the slope is negative, the disturbance will tend to decrease. Figure 11 and Figure 12 show that all the values of damping coefficients are positive, showing dynamic instability for all configurations at all mean angles of attack. It means that the disturbances will increase with time and will not decay. Therefore, counter measurements need to be taken to overcome dynamic instability. Dynamic instability is highly undesirable in civil aviation. Another observation that can be made is that magnitude of damping coefficients increases with an increase in mean angles of attack, pointing that the higher the mean angles of attack, the more dynamically unstable it is.

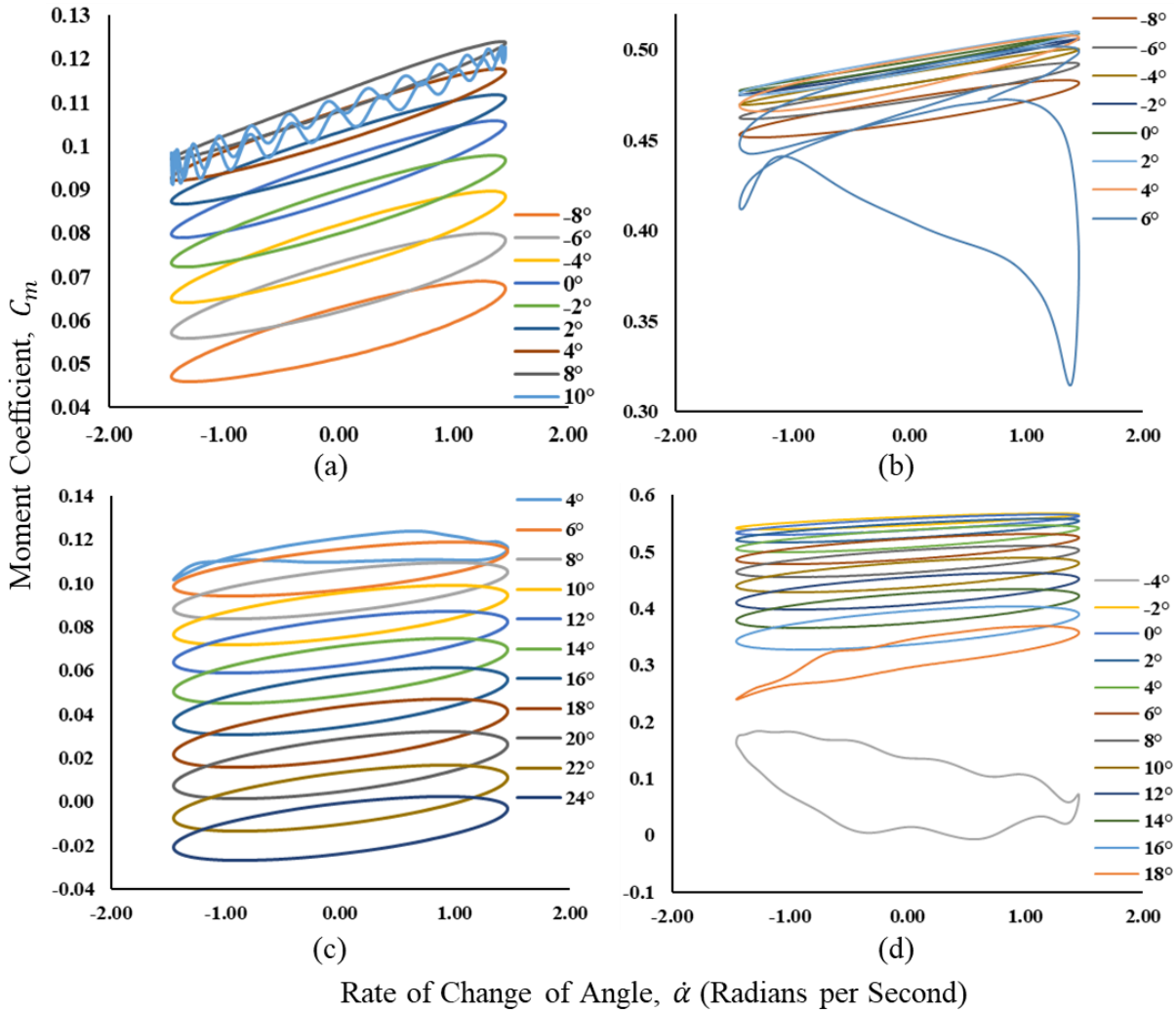


Figure 11 – Moment coefficients vs rate of change of angle of attack (in radians) for (a) clean configuration (b) flap deployed configuration (c) slat deployed configuration (d) slat and flap deployed configuration.

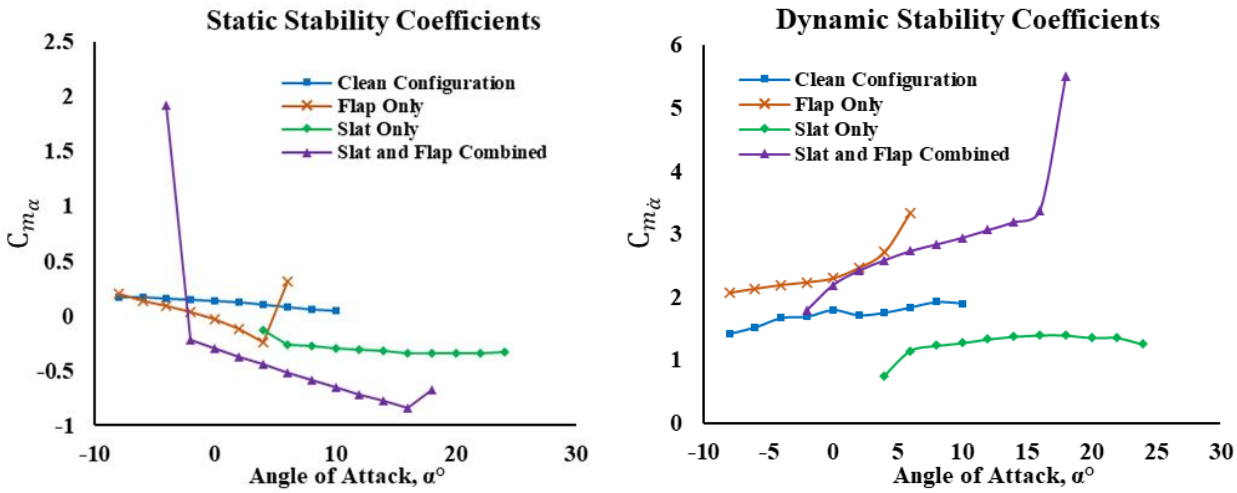


Figure 12 – (a) Static and (b) dynamic stability coefficients for different configurations

## 4. Conclusion

Steady flow analysis over TC12 airfoil with clean configuration and the high-lift configuration was carried out with different turbulent models, and the results are validated by comparing with experimental data. Among those, the S-A model showed a better approximation of experimental results. For stability derivatives, validation of experimental data was carried out with simulated flow over oscillating NACA 0012 airfoil. First, the approximate time step was found by decreasing the time step until convergence. Two turbulence models – S-A and k-ω were used in this case, and both gave the same results. S-A turbulence model was chosen because it is less computationally expensive. The same procedure was used to derive stability derivatives' coefficients of clean and high-lift configurations of TC12 airfoil.

Static stability derivatives' coefficients for all configurations at different mean angles of attack are presented. These coefficients are related to flow physics. It can be concluded that instabilities occur due to the position of the center of pressure and the vortices generated at certain angles of attack. It is observed that clean configuration is statically unstable at all chosen ranges of mean angles of attack. At the same time, the only flap deployed is statically unstable at negative angles of attack. It remains stable at positive angles of attack before flow separation at a 6° mean angle of attack. The slat-only deployed configuration remains stable between 4° and 24°. The slat and flap deployed configuration is unstable at a -4° angle of attack due to separated flow on the lower surface of the airfoil and becomes statically stable at a -2° angle of attack.

The values of damping coefficients for all configurations are positive, proving that if the airfoil is perturbed with a wind gust or due to any other disturbance in the pitch direction, the oscillation will not decay and will tend to increase with time, hence dynamically unstable.

## 5. Contact Author Email Address

adnan@rcms.nust.edu.pk

## 6. Copyright Statement



## References

[1] A. M. O. Smith, "High-lift aerodynamics," *J. Aircr.*, vol. 12, no. 6, pp. 501–530, 1975.
[2] P. K. C. Rudolph, "High-lift systems on commercial subsonic airliners," 1996.
[3] J. Meseguer, S. Franchini, I. Pérez-Grande, and J. L. Sanz, "On the aerodynamics of leading-edge high-lift devices of avian wings," *Proc. Inst. Mech. Eng. Part G J. Aerosp. Eng.*, vol. 219, no. 1, pp. 63–68,

2005.
[4] R. W. Gallington and H. R. Chaplin, “Theory of Power Augmented Ram Lift at Zero Forward Speed,” DAVID W TAYLOR NAVAL SHIP RESEARCH AND DEVELOPMENT CENTER BETHESDA MD …, 1976.
[5] A. Seifert, T. Bachar, D. Koss, M. Shepshelovich, and I. Wygnanski, “Oscillatory blowing: a tool to delay boundary-layer separation,” *AIAA J.*, vol. 31, no. 11, pp. 2052–2060, 1993.
[6] M. B. Bragg and G. M. Gregorek, “Experimental study of airfoil performance with vortex generators,” *J. Aircr.*, vol. 24, no. 5, pp. 305–309, 1987.
[7] B. R. White and J. C. Schulz, “Magnus effect in saltation,” *J. Fluid Mech.*, vol. 81, no. 3, pp. 497–512, 1977.
[8] J. Little and M. Samimy, “High-lift airfoil separation with dielectric barrier discharge plasma actuation,” *AIAA J.*, vol. 48, no. 12, pp. 2884–2898, 2010.
[9] L. A. T. de Vargas and P. H. I. A. de Oliveira, “A fast aerodynamic procedure for a complete aircraft design using the know airfoil characteristics,” SAE Technical Paper, 2006.
[10] A. Jameson, “Optimum aerodynamic design using CFD and control theory,” in *12th computational fluid dynamics conference*, 1995, p. 1729.
[11] E. TINOCO, “The role of computational fluid dynamics (CFD) in aircraft design,” in *Aerospace Engineering Conference and Show*, p. 1801.
[12] W. L. Oberkampf and T. G. Trucano, “Verification and validation in computational fluid dynamics,” *Prog. Aerosp. Sci.*, vol. 38, no. 3, pp. 209–272, 2002.
[13] E. Torenbeek, *Advanced aircraft design: conceptual design, analysis and optimization of subsonic civil airplanes*. John Wiley & Sons, 2013.
[14] B. N. Pamadi, *Performance, stability, dynamics, and control of airplanes*. American Institute of aeronautics and astronautics, 2004.
[15] M. Sadraey, “Automatic Flight Control Systems,” *Synth. Lect. Mech. Eng.*, vol. 4, no. 1, pp. 1–173, 2020.
[16] A. Da Ronch, D. Vallespin, M. Ghoreyshi, and K. J. Badcock, “Evaluation of dynamic derivatives using computational fluid dynamics,” *AIAA J.*, vol. 50, no. 2, pp. 470–484, 2012.
[17] N. Alemdaroglu, I. Iyigun, M. Altun, H. Uysal, F. Quagliotti, and G. Guglieri, “Determination of dynamic stability derivatives using forced oscillation technique,” in *40th AIAA Aerospace Sciences Meeting & Exhibit*, 2002, p. 528.
[18] R. H. Landon, “NACA 0012. Oscillating and transient pitching,” *Data Set*, vol. 3, 1982.
[19] J. D. M. Botha, L. Dala, and S. Schaber, “Optimisation of a novel trailing edge concept for a high lift device,” *Adv. Aircr. Spacecr. Sci.*, vol. 2, no. 3, p. 329, 2015.
[20] P. Spalart and S. Allmaras, “A one-equation turbulence model for aerodynamic flows,” in *30th aerospace sciences meeting and exhibit*, 1992, p. 439.
[21] M. M. Koochesfahani, “Vortical patterns in the wake of an oscillating airfoil,” *AIAA J.*, vol. 27, no. 9, pp. 1200–1205, 1989.
[22] M. S. Mumtaz, A. Maqsood, and S. Sherbaz, “Computational modeling of dynamic stability derivatives for generic airfoils,” in *MATEC Web of Conferences*, 2017, vol. 95, p. 12006.
[23] S. Rashid, F. Nawaz, A. Maqsood, R. Riaz, and S. Salamat, “Shock reduction through opposing jets—Aerodynamic performance and flight stability perspectives,” *Appl. Sci.*, vol. 10, no. 1, p. 180, 2020.
[24] K. Willcox, “Unsteady flow sensing and estimation via the gappy proper orthogonal decomposition,” *Comput. Fluids*, vol. 35, no. 2, pp. 208–226, 2006.
[25] K. Gharali and D. A. Johnson, “Numerical modeling of an S809 airfoil under dynamic stall, erosion and high reduced frequencies,” *Appl. Energy*, vol. 93, pp. 45–52, 2012.
[26] A. Fluent, “Ansys fluent udf manual,” *ANSYS Inc., USA*, 2015.
[27] H. Muhammad Umer, A. Maqsood, R. Riaz, and S. Salamat, “Stability Characteristics of Wing Span and Sweep Morphing for Small Unmanned Air Vehicle: A Mathematical Analysis,” *Math. Probl. Eng.*, vol. 2020, 2020.
[28] M. V Cook, *Flight dynamics principles: a linear systems approach to aircraft stability and control*. Butterworth-Heinemann, 2012.
[29] M. E. Bartowitz, “Determination of Static and Dynamic Stability Derivatives Using Beggar,” AIR FORCE INSTITUTE OF TECHNOLOGY WRIGHT-PATTERSON AFB OH GRADUATE SCHOOL OF …, 2008.